Li et al. Nanoscale Research Letters (2015) 10:418
DOI 10.1186/s11671-015-1129-3

Nanoscale Research Letters
a SpringerOpen Journal

NANO EXPRESS Open Access

Enhance photoelectrochemical hydrogen-generation activity and stability of TiO_2 nanorod arrays sensitized by PbS and CdS quantum dots under UV-visible light

Lei Li[1], Haitao Dai[1*], Liefeng Feng[1], Dan Luo[2], Shuguo Wang[1] and Xiaowei Sun[3*]

Abstract

We develop a composite photoanode by sensitizing TiO_2 nanorod arrays with PbS quantum dots (QDs) and CdS QDs. Benefitted from additional introduced PbS QDs and CdS QDs onto TiO_2, the absorption of the composite photoanodes are broaden from UV to visible region. The experimental results showed that the PbS sandwiched between TiO_2 and CdS cannot only broad the absorption properties but also improve the stability. The stability can be explained by the hole facile transmission from PbS to CdS because of the valence band offsets between PbS and CdS which cause a small energy barrier and reduce the hole accumulation. The photocurrent density reached 1.35 mA cm^{-2} at 0.9716 V vs. RHE (0 V vs. Ag/AgCl, under 60 mW cm^{-2} illumination) for TiO_2/PbS/CdS. The highest photocurrent of TiO_2/PbS/CdS can be explained by the smallest of total resistance (138 Ω cm^{-2}) compared to TiO_2/CdS and pristine TiO_2.

Keywords: Photoelectrochemical, Solar water splitting, Hydrogen generation

PACS: 8200008245+z, 8250Fv

Background

Energy crisis is one of the great challenges of the twenty-first century facing humankind due to the excessive dependence on fossil fuels. Solar energy, as a renewable and almost inexhaustible energy, is expected as one promising candidate to resolve the upcoming crisis. Solar energy can be utilized via a variety of fashions, such as solar cells [1], photoelectrochemical (PEC) device for hydrogen production [2], thermal energy storage [3], and so on [4]. Hydrogen energy, as a clean energy, has been a promising candidate for next-generation energy. Especially, after Fujishima and Honda found the direct hydrogen generation by solar water splitting with TiO_2 photoanode in 1972, PEC cells based on TiO_2 for solar hydrogen production have been studied extensively [5–9]. This method paves a way to generate clean hydrogen energy by means of almost inexhaustible solar energy to split water (most abundant materials in Earth) mediated with wide bandgap semiconductor TiO_2 (suitable bandgap, chemical stability, cost effectiveness, and environmental friendliness [10, 11]). However, the performance of devices based on wide bandgap semiconductor (ZnO, TiO_2, etc.) is limited by the narrow absorption range. For TiO_2 (3.0 eV for rutile TiO_2, 3.2 eV for anatase TiO_2), only UV light, which carries about 4 % power of sunlight, can be effectively utilized which also limits the performance of PEC for hydrogen generation. To enhance or broaden the absorption region of TiO_2, massive methods have been explored, for example, introducing proper dopants [10–13] and increasing specific surface area [14]. Among them, sensitizing the narrow bandgap semiconductor such as CdS [15–19], CdSe [13, 15, 16], Bi_2S_3 [20], PbS [17, 21, 22], and CdTe [23] with TiO_2 to broaden the visible absorption is emerging as an effective method. Narrow bandgap mental

* Correspondence: htdai@tju.edu.cn; exwsun@ntu.edu.sg
[1]Tianjin Key Laboratory of Low Dimensional Materials Physics and Preparing Technology, School of Science, Tianjin University, Tianjin 300072, China
[3]Nanyang Technological University, School of Electrical and Electronic Engineering, LUMINOUS! Centre of Excellence for Semiconductor Lighting and Displays, Singapore 639798, Singapore
Full list of author information is available at the end of the article

sulfide, such as CdS and PbS, has been investigated comprehensively for application in solar-to-hydrogen due to the considerable absorption in visible and near-infrared spectrum [24–30]. However, narrow bandgap of PbS lead oxidation of S^{2-} attributed to hole accumulation, which causes photo-corrosion and decreases the stability of devices [26, 31].

In the present work, we prepared the heterojunction of PbS QDs and CdS QDs by means of the successive ionic layer absorption and reaction (SILAR) process on TiO_2 nanorod arrays. Experimental results show that fabricated photoanode based on TiO_2 nanorod arrays sensitized with the PbS/CdS heterojunction could improve UV-visible absorption and boost the photocurrent density. Meanwhile, due to valence band offsets between PbS and CdS, the hole accumulation is reduced, which improved the stability of TiO_2/PbS/CdS photoanode.

Methods

Preparation of Photoanodes

TiO_2 nanorod arrays were prepared on FTO glass initially based on conventional solvent-based method [20]. The cleaned FTO substrate was placed upside down in a sealed Teflon reactor filled with hydrochloric acid (15 mL), deionized water (15 mL), and titanium *n*-butoxide (0.5 mL) at 150 °C for 8 h. After the reaction, the FTO substrate was taken out, rinsed with deionized water, and dried in ambient air. To sensitize PbS and CdS QDs, the FTO substrate covered with TiO_2 nanorod arrays were sequentially dipped into various precursor solutions ($Cd(Ac)_2$, $Pb(Ac)_2$, and Na_2S). First, the TiO_2 nanorods with FTO substrate were immersed into 0.02 M methanolic solution of lead acetate ($Pb(Ac)_2$) and 0.02 M solution of $Na_2S \cdot 9H_2O$ in methanol-water (1:1, *v*/*v*). After rinsing with methanol, PbS QDs are sensitized on TiO_2 nanorods. At last, the substrate is dipped into the 0.05 M precursor solution of Cd^{2+} and S^{2-} to prepare CdS QDs.

Characterization

In our experiments, three samples are prepared, i.e., pristine TiO2, TiO_2/CdS, and TiO_2/PbS/CdS, for performance comparison. The morphologies are observed with a field-emission scanning electron microscopy (SEM, Hitachi, S-4800) and transmission electron microscopy equipped with an energy-dispersive X-ray spectroscopy (EDS) (TEM, JEM-2100F). The UV-visible absorption spectra are measured with a spectrometer (UV-3600, Shimadzu) under diffuse reflection method. The crystalline phase was recorded by X-ray diffraction (XRD) patterns, with a two theta value range from 10° to 90°, at 5°/min (Rigaku, D/MAX-2500). X-ray photoelectron spectroscopy (XPS) was measured on Thermo Scientific Theta Probe XPS.

Evaluation PEC Performance

The PEC properties are studied with an electrochemical workstation (CHI660D) with a three-electrode system in 0.35 M Na_2SO_3 and 0.25 M Na_2S (PH = 13) electrolyte solution at room temperature. The substrate, Pt mesh, and Ag/AgCl electrode are used as working electrode, counter electrode, and reference electrode, respectively. A 150 W Xenon light source with AM1.5 filter is used to irradiate to the substrate, and the power of the solar simulator is measured to be 60 $mW \cdot cm^{-2}$. The linear sweep voltammetry (LSV) is recorded at a scan rate 10 mV/s, with chopped AM1.5G simulated sunlight irradiation. *I*–*t* curves were measured at 0.9716 V vs. RHE under AM1.5 irradiation. Electrochemical impedance spectroscopy (EIS) was measured from 1 Hz to 100 kHz, with AC amplitude of 5 mV. IPCE measurements were taken with a tungsten light and monochromator (a standard silicon cell as a reference).

Results and Discussion

First, the morphologies, structures, and crystalline phases of the composite system are investigated via FESEM and XRD shown in Fig. 1a–d. According to Fig. 1a, the fabricated TiO_2 nanorod arrays covered the FTO glass uniformly. The diameter of the TiO_2 nanorod is about 110 nm. Figure 1b shows the cross-section FESEM image of TiO_2 nanorod arrays. The length of the TiO_2 nanorod is about 3 μm. After depositing PbS QDs and CdS QDs, we can see that the QDs cover the nanorod arrays with large area from the cross-section FESEM image shown in Fig. 1c. The XRD patterns of TiO_2/PbS/CdS are recorded in Fig. 1d. The diffraction peaks corresponding to SnO_2 are attributed to FTO glass. The diffraction peaks are located at the $2\theta = 36.1°$ and 62.7° corresponding to rutile TiO_2 phase. $2\theta = 30.1°$ and 69.1° corresponding to PbS phase. The diffraction peaks are located at the $2\theta = 70.4°$ corresponding to CdS phase [32]. The diffraction peaks of CdS phase is not easy to find, because some peaks are located very close to SnO_2, such as $2\theta = 26.23°$ and 52.06° [2].

To further prove crystalline phase, the HRTEM and EDS were investigated and shown in Fig. 2. According to inset of Fig. 2a, the EDS of the nanostructure of the Ti, O, Cd, Pb, and S elements are mainly from TiO_2, CdS, and PbS. C element is from the carbon film of Cu mesh. Figure 2b shows the HRTEM of the marked area in Fig. 2a. The *d*-spacing of (001) and (110) in Fig. 2b is consistent with rutile TiO_2, which are 0.29 and 0.32 nm, respectively. The $d(111) = 0.34$ nm is consistent with rock salt PbS. The $d(101) = 0.32$ nm of CdS is shown in Fig. 2b.

The TiO_2/PbS/CdS sample was further investigated by XPS spectrum shown in Fig. 3. In Fig. 3a, the photoelectron peaks of Pb 4f can be observed at 137.4 and 142.2 eV, which comes from Pb^{2+} ions of PbS QDs [28]. Figure 3b

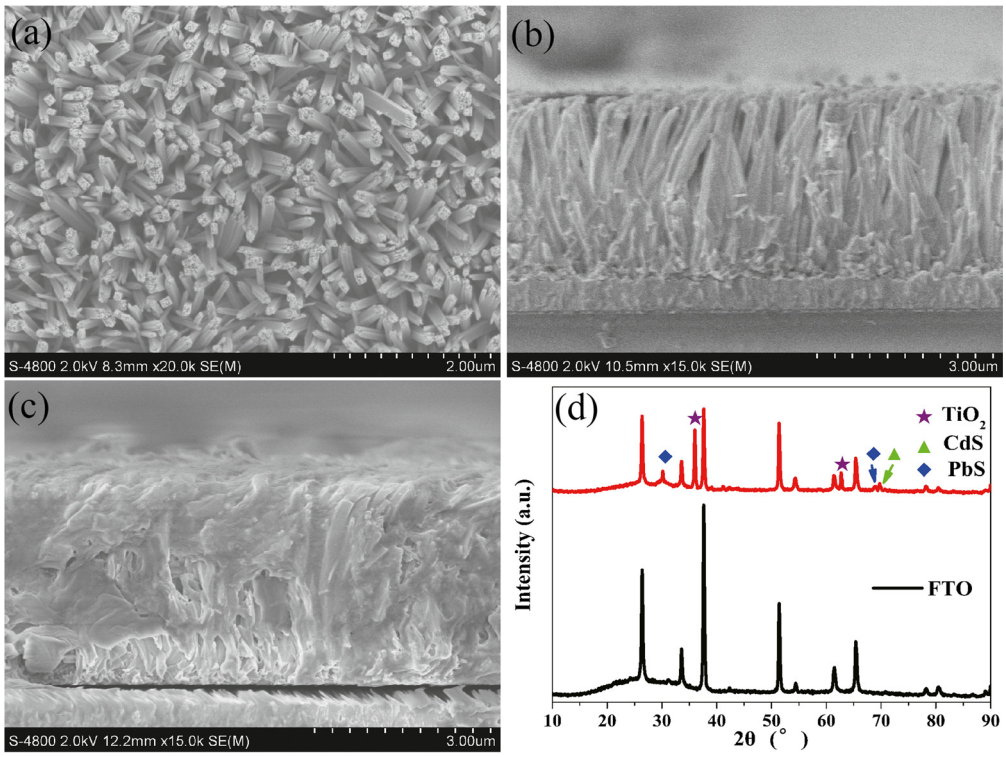

Fig. 1 The top (**a**) and cross-section (**b**) FESEM images of pristine TiO_2. The cross-section FESEM of TiO_2 (**c**) after depositing PbS and CdS QDS. XRD patterns (**d**) of FTO glass and TiO_2/PbS/CdS

shows the Cd 3d peaks at 404.7 and 411.4 eV, which originates from Cd^{2+} ions of the CdS QDs [33, 34]. In Fig. 3c, the S 2p peaks at 161.0 and 162.2 eV can be assigned to the sulfide of PbS and CdS QDs. Therefore, PbS QDs and CdS QDs are decorated successfully on TiO_2 nanorod arrays, which are verified by the XRD patterns, EDS, HRTEM, and XPS.

The optical absorption behavior was illustrated in Fig. 4a. It is obvious that the absorption of TiO_2/PbS/CdS is enhanced in visible spectrum in comparison with

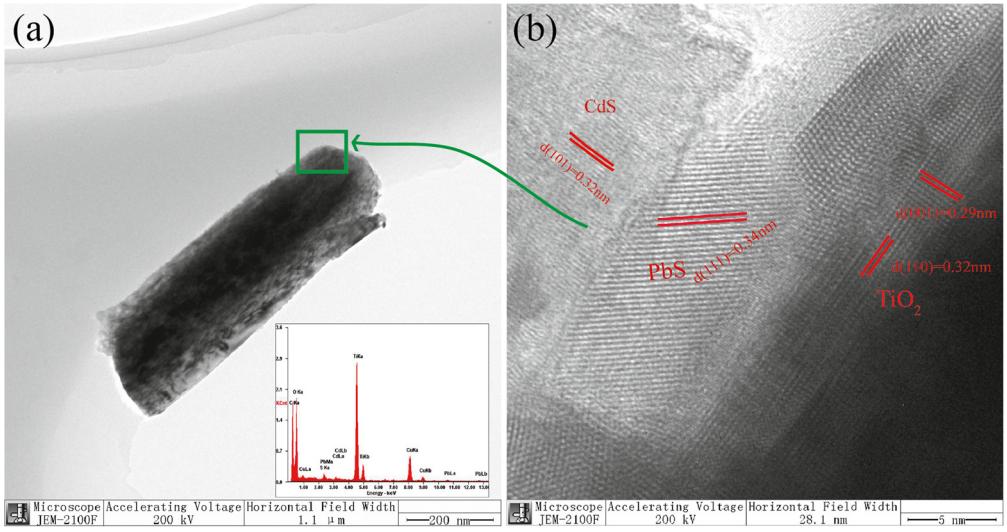

Fig. 2 TEM image and EDS (**a**) of TiO_2/PbS/CdS. HRTEM image (**b**) of marked area in (**a**)

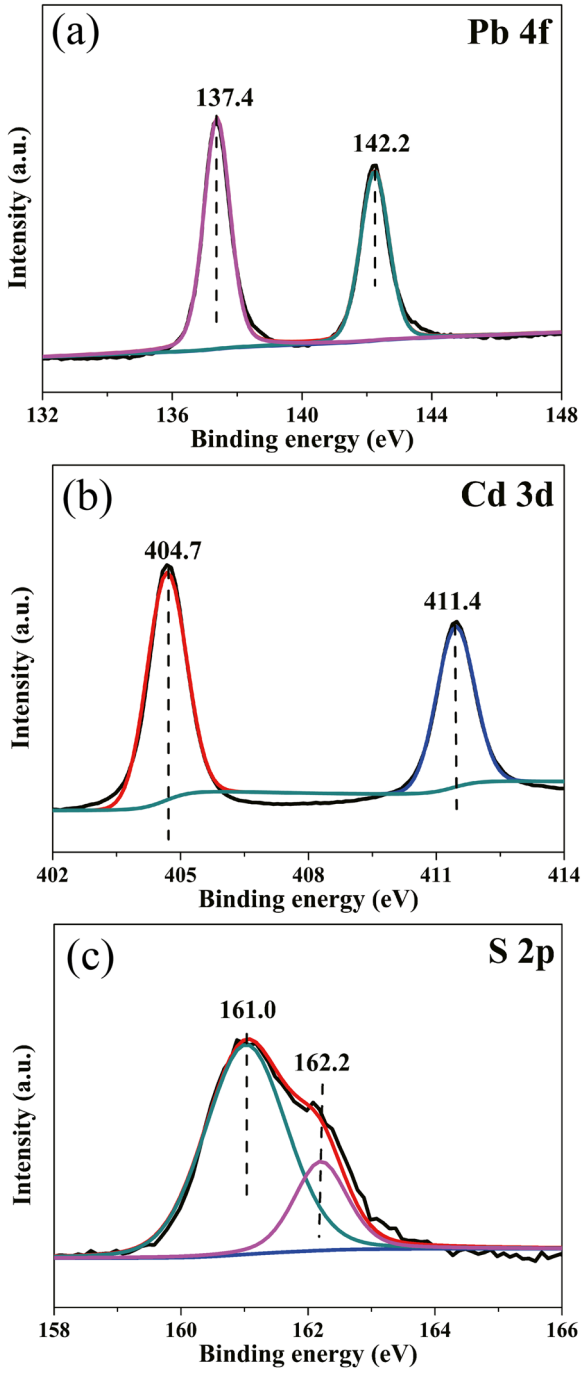

Fig. 3 XPS curves of Pb 4f (**a**), Cd 3d (**b**), and S2p (**c**)

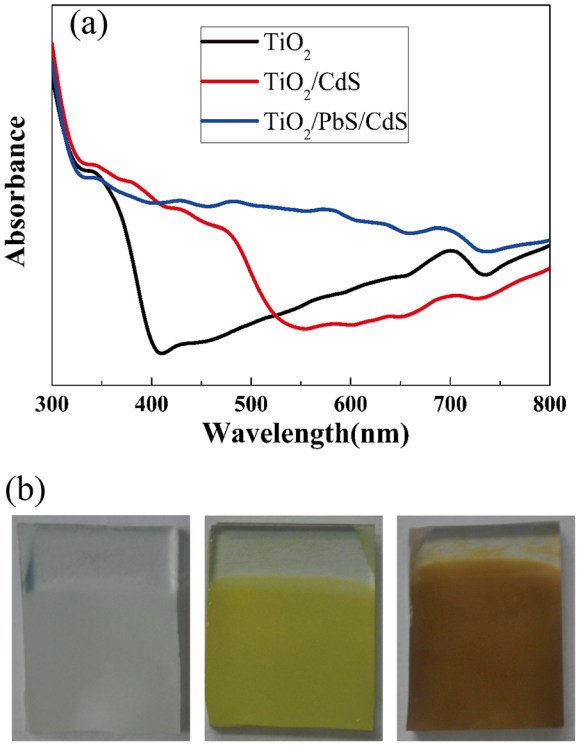

Fig. 4 UV-visible absorption spectrum (**a**) and photograph (**b**) of pristine TiO_2, TiO_2/CdS, and TiO_2/PbS/CdS

pristine TiO_2 and TiO_2/CdS. The photograph of pristine TiO_2, TiO_2/CdS, and TiO_2/PbS/CdS is shown in Fig. 4b. The white color of pristine TiO_2 is shown to be absorption free in visible light. As CdS is sensitized, the yellow color implies the enhanced absorption in visible light. The brown-black color after sensitized PbS shows the stronger absorption in visible light.

To characterize the PEC properties of fabricated photoanodes, a three-electrode setup is used, which is shined by 150 W Xeon light source (with AM1.5 filter and 60 mW/cm^2 power). The details of LSV curves with chopped illumination are shown in Fig. 5a. The current density is only 0.09 mA cm^{-2} for pristine TiO_2 at 0.9716 V vs. RHE (0 V vs. Ag/AgCl). For TiO_2/CdS, the current density increases to 0.72 mA cm^{-2} at 0.9716 V vs. RHE. The current density boosts to 1.35 mA cm^{-2} at 0.9716 V vs. RHE for TiO_2/PbS/CdS, which is ascribed to the enhanced UV-visible absorption. The series of spikes located at the on or off edges of the curves indicate carrier accumulation at the electrode–electrolyte interface and slow oxygen evolving reaction kinetics [16, 20, 35]. Figure 5b shows the *I*–*t* curves at 0.9716 V vs. RHE under AM1.5 illumination. The current density of TiO_2/PbS/CdS is highest compared with pristine TiO_2 and TiO_2/CdS. However, the TiO_2/PbS/CdS sample shows more stability than sensitized PbS only [31]. This phenomenon can be attributed to the valence band (VB) offsets between PbS and CdS shown in Fig. 5c, which cause small energy barrier, allowing facile hole transmission from PbS to CdS and preventing the hole accumulation from oxidizing PbS and CdS [36]. From Fig. 5d, the IPCE curve of TiO_2/PbS/CdS clearly shows the widened UV-visible light absorption region compared to TiO_2/CdS, even though the IPCE of TiO_2/CdS is higher than TiO_2/PbS/CdS under the

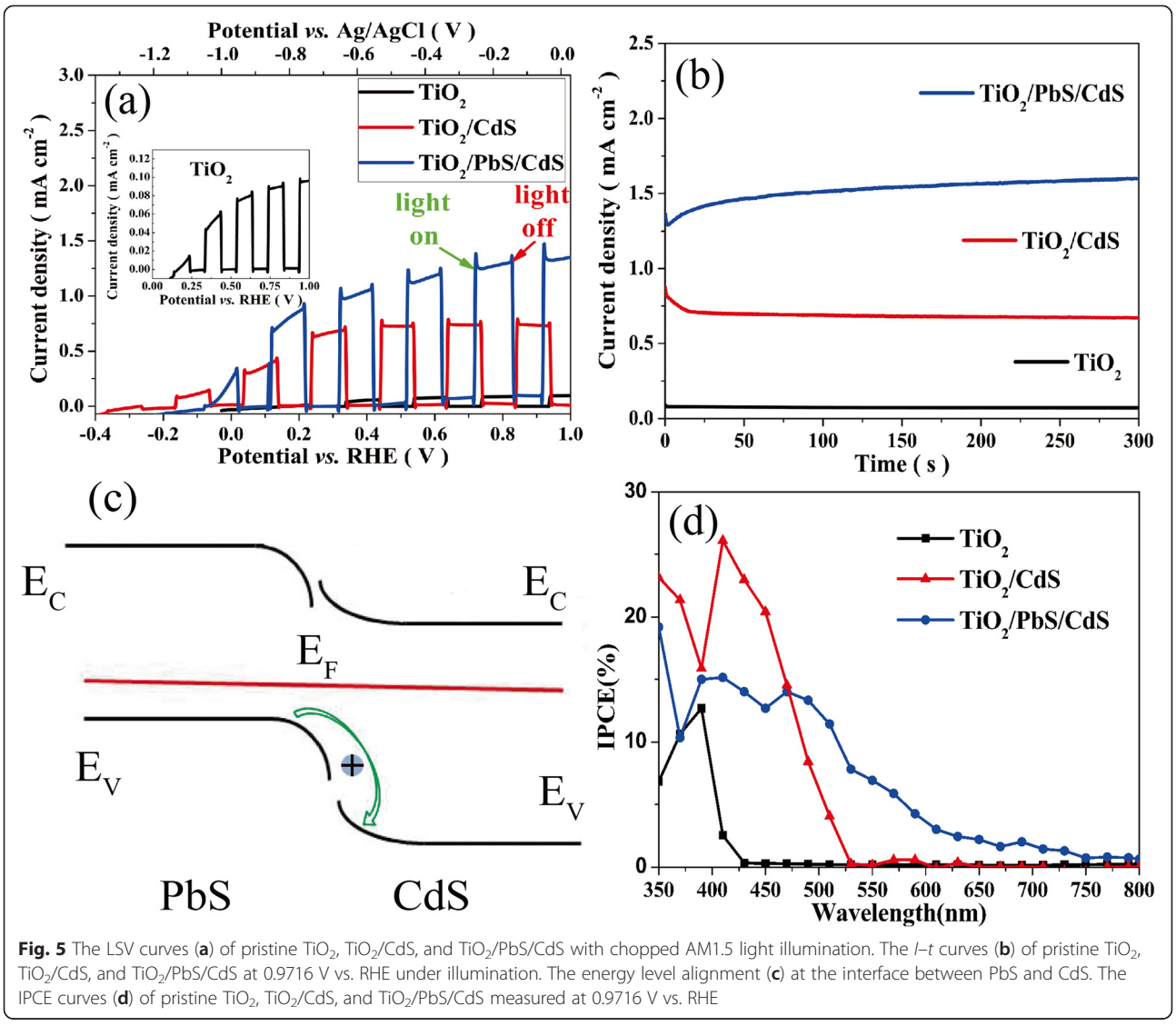

Fig. 5 The LSV curves (**a**) of pristine TiO_2, TiO_2/CdS, and TiO_2/PbS/CdS with chopped AM1.5 light illumination. The *I–t* curves (**b**) of pristine TiO_2, TiO_2/CdS, and TiO_2/PbS/CdS at 0.9716 V vs. RHE under illumination. The energy level alignment (**c**) at the interface between PbS and CdS. The IPCE curves (**d**) of pristine TiO_2, TiO_2/CdS, and TiO_2/PbS/CdS measured at 0.9716 V vs. RHE

wavelength of 472 nm. Therefore, the photoanode with TiO_2/PbS/CdS showed an enhanced PEC performance.

In order to further investigate the underlying reason for the enhanced PEC performance of fabricated composite photoanodes, the impedance spectroscopy (EIS) of different samples and the equivalent circuit have been shown in Fig. 6. For the equivalent circuit, R_s is the series resistance, R_{dl} and C_{dl} are the resistance and capacitance in the semiconductor, and R_H and C_H are the resistance and capacitance at the Helmholtz double layer [37]. As can be seen, the corresponding radii of semicircles (EIS) for pristine TiO_2, TiO_2/CdS, and TiO_2/PbS/CdS decrease sequentially. The smallest radii of the semicircles for TiO_2/PbS/CdS compared with pristine TiO_2 and TiO_2/CdS mean the smallest charge-transfer impedance [38]. Also, the PEC performance can be explained by the value of total resistance ($R_t = R_S + R_H + R_{dl}$) [39]. The R_t value for pristine TiO_2 is 5651 Ω cm^{-2}, for TiO_2/CdS is 233 Ω cm^{-2}, and for TiO_2/PbS/CdS is 138 Ω cm^{-2}. The lowest R_t results in the highest photocurrent for TiO_2/PbS/CdS compared with TiO_2/CdS and pristine TiO_2.

Conclusions

The composite photoanode for solar water splitting with sandwiched structures (TiO_2/PbS/CdS) was prepared by means of facile SILAR method. By introducing PbS QDs between TiO_2 nanorod arrays and CdS QDs, both the absorption efficiency and stability are improved for the fabricated PEC cell. The highest photocurrent density (1.35 mA cm^{-2} at 0.9716 V vs. RHE) is achieved with TiO_2/PbS/CdS structure compared to that of pristine TiO_2 and TiO_2/CdS. At the same time, the PEC cell of TiO_2/PbS/CdS is stablest under light illumination. The

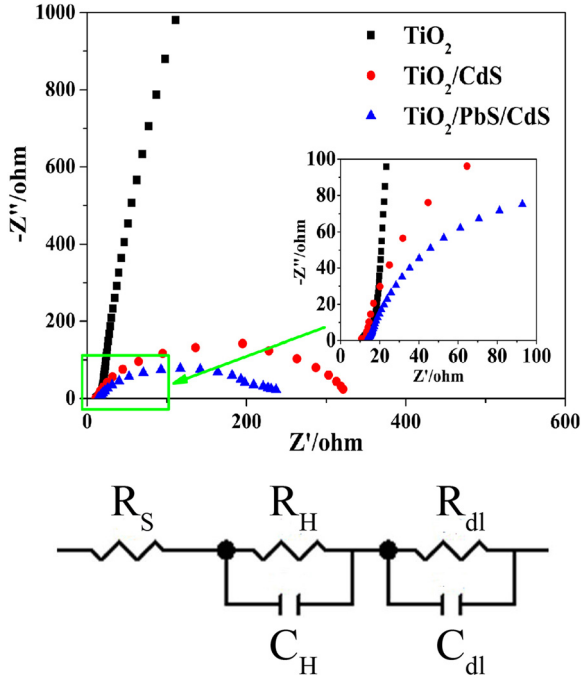

Fig. 6 EIS of and equivalent circuit pristine TiO_2, TiO_2/CdS, and TiO_2/PbS/CdS

enhanced performance is attributed to the VB offsets between PbS and CdS, which allow facile hole transmission from PbS to CdS leading to high photon current and photo-corrosion resistance. This structure presents a promising roadmap for high performance and stability devices in solar usage field.

Competing interests
The authors declare that they have no competing interests.

Authors' contributions
LL and HTD were involved in the design, development of materials, photoelectrochemical measurements, and manuscript writing. LFF, DL, and SGW performed the XPS SEM, TEM, and optical characterization. XWS helped to draft the manuscript. All authors read and approved the final manuscript.

Acknowledgements
This work was supported in part by the National Natural Science Foundation (Grant Nos. 61177061,11204208, and 61405088); the Open Research Fund of the State Key Laboratory of Transient Optics and Photonics (China Academy of Sciences); and key project of Nature Science Foundation of Tianjin No. 14JCZDJC31400.

Author details
[1]Tianjin Key Laboratory of Low Dimensional Materials Physics and Preparing Technology, School of Science, Tianjin University, Tianjin 300072, China. [2]Department of Electrical and Electronic Engineering, South University of Science and Technology of China, Shenzhen 518055, China. [3]Nanyang Technological University, School of Electrical and Electronic Engineering, LUMINOUS! Centre of Excellence for Semiconductor Lighting and Displays, Singapore 639798, Singapore.

Received: 1 August 2015 Accepted: 16 October 2015
Published online: 26 October 2015

References
1. Leijtens T, Eperon GE, Pathak S, Abate A, Lee MM, Snaith HJ (2013) Overcoming ultraviolet light instability of sensitized TiO_2 with meso-superstructured organometal tri-halide perovskite solar cells. Nat Commun 4:2885–2893
2. Hossain MA, Koh ZY, Wang Q (2012) PbS/CdS-sensitized mesoscopic SnO_2 solar cells for enhanced infrared light harnessing. Phys Chem Chem Phys 14:7367–7374
3. Khaselev O (1988) A monolithic photovoltaic-photoelectrochemical device for hydrogen production via water splitting. Science 280:425–427
4. Sharma A, Tyagi VV, Chen CR, Buddhi D (2009) Review on thermal energy storage with phase change materials and applications. Renew Sust Energy Rev 13:318–345
5. Fujishima A, Honda K (1972) Electrochemical photolysis of water at a semiconductor electrode. Nature 238:37–38
6. Nguyen NT, Altomare M, Yoo JE (2015) Efficient photocatalytic H_2 evolution: controlled dewetting–dealloying to fabricate site-selective high-activity nanoporous Au particles on highly ordered TiO_2 nanotube arrays. Adv Mater 27:3208–3215
7. Learyand R, Westwood A (2011) Carbonaceous nanomaterials for the enhancement of TiO_2 photocatalysis. Carbon 49:741–772
8. Fujishima A, Zhang XT, Trylc DA (2008) TiO_2 photocatalysis and related surface phenomena. Surf Sci Rep 63:515–582
9. Xiang QJ, Yu JG, Jaroniec M (2012) Synergetic effect of MoS_2 and graphene as cocatalysts for enhanced photocatalytic H_2 production activity of TiO_2 nanoparticles. J Am Chem Soc 134:6575–6578
10. Park JH, Kim S, Bard AJ (2006) Novel carbon-doped TiO_2 nanotube arrays with high aspect ratios for efficient solar water splitting. Nano Lett 6:24–28
11. Liu SJ, Yu JG, Jaroniec M (2011) Anatase TiO_2 with dominant high-energy {001} facets: synthesis, properties, and applications. Chem Mater 23:4085–4093
12. Yu JC, Yu JG, Ho W, Jiang Z, Zhang LZ (2002) Effects of F-doping on the photocatalytic activity and microstructures of nanocrystalline TiO_2 powders. Chem Mater 14:3808–3816
13. Li X, Yu JG, Low JX, Fang YP, Xiao J, Chen XB (2015) Engineering heterogeneous semiconductors for solar water splitting. J Mater Chem A 3:2485–2534
14. Cho IS, Chen ZB, Forman AJ, Kim DR, Rao PM, Jaramillo TF, Zheng X (2011) Branched TiO_2 nanorods for photoelectrochemical hydrogen production. Nano Lett 11:4978–4984
15. Das K, De SK (2009) Optical properties of the type-II core-shell TiO_2@CdS nanorods for photovoltaic applications. J Phys Chem C 113:3494–3501
16. Luo JS, Ma L, He T, Ng CF, Wang SH, Sun HD, Fan HJ (2012) TiO_2/(CdS, CdSe, CdSeS) nanorod heterostructures and photoelectrochemical properties. J Phys Chem C 116:11956–11963
17. Yang J, Yan H, Wang X, Wen F, Wang Z, Fan D, Shi JY, Li C (2012) Roles of cocatalysts in Pt-PdS/CdS with exceptionally high quantum efficiency for photocatalytic hydrogen production. J Catal 290:151–157
18. Zeng QY, Li XJ, Xi M, Wu LP, Xu Z, Zhou ZY (2013) Fabrication of TiO_2/CdS/TiO_2 nanotube/Ti mesh electrode and application in photoelectrocatalytic cell system for degradation of methylene blue under visible light illumination. Asian J Chem 25:8527–8532
19. Long LZ, Yu X, Wu LP, Li J, Li XJ (2014) Nano-CdS confined within titanate nanotubes for efficient photocatalytic hydrogen production under visible light illumination. Nanotechnology 25:035603
20. Ai GJ, Mo R, Chen Q, Xu H, Yang S, Li HX, Zhong JX (2015) TiO_2/Bi_2S_3 core-shell nanowire arrays for photoelectrochemical hydrogen generation. RSC Adv 5:13544–13549
21. Buatong N, Tang IM, Pon-On W (2015) Quantum dot-sensitized solar cells having 3D-TiO_2 flower-like structures on the surface of titania nanorods with CuS counter electrode. Nanoscale Res Lett 10:146–156
22. Yan HJ, Yang JH, Ma GJ, Wu GP, Zong X, Lei ZB, Shi JY, Li C (2009) Visible-light-driven hydrogen production with extremely high quantum efficiency on Pt-PdS/CdS photocatalyst. J Catal 266:165–168
23. Chen HM, Chen CK, Chang YC, Tsai CW, Liu RS, Hu SF, Chang WS, Chen KH (2010) Quantum dot monolayer sensitized ZnO nanowire-array photoelectrodes: true efficiency for water splitting. Angew Chem 122:6102–6105
24. Huang L, Wang XL, Yang JH, Liu G, Han JF, Li C (2013) Dual cocatalysts loaded Type I CdS/ZnS core/shell nanocrystals as effective and stable photocatalysts for H_2 evolution. J Phys Chem C 117:11584–11591

25. Trevisan R, Rodenas P, Gonzalez-Pedro V, Sima C, Sanchez RS, Barea EM, Mora-Sero I, Fabregat-Santiago F, Gimenez S (2013) Harnessing infrared photons for photoelectrochemical hydrogen generation. A PbS quantum dot based "quasi-artificial leaf". J Phys Chem Lett 4:141–146.
26. Lian Z, Xu PP, Wang WC, Zhang DQ, Xiao SN, Li X, Li GS (2015) C_{60} decorated CdS/TiO_2 mesoporous architectures with enhanced photostability and photocatalytic activity for H_2 evolution. ACS Appl Mater Interfaces 7:4533–4540.
27. Zhang XL, Li Y, Zhao JL, Wang SG, Li YD, Dai HT, Sun XW (2014) Advanced three-component ZnO/Ag/CdS nanocomposite photoanode for photocatalytic water splitting. J Power Sources 269:466–472.
28. Bhandari KP, Choi H, Jeong S, Mahabaduge H, Ellingson RJ (2014) Determination of heterojunction band offsets between CdS bulk and PbS quantum dots using photoelectron spectroscopy. Appl Phys Lett 105:131604–131608
29. Li Q, Li X, Wageh S, Al-Ghamdi AA, Yu JG (2015) CdS/Graphene nanocomposite photocatalysts. Adv Energy Mater 5:1500010
30. Chen J, Wu XJ, Yin LS, Li B, Hong X, Fan ZX, Chen B, Xue C, Zhang H (2015) One-pot synthesis of CdS nanocrystals hybridized with single-layer transition-metal dichalcogenide nanosheets for efficient photocatalytic hydrogen evolution. Angew Chem Int Ed 54:1210–1214.
31. Yang SM, Wang ZS, Huang CH (2001) The photoelectrochemical properties of TiO_2 electrodes modified by quantum size PbS and thoils. Synthetic Met 123:267–272
32. Long LZ, Li J, Wu LP, Li XJ (2014) Enhanced photocatalytic performance of platinized CdS/TiO_2 by optimizing calcination temperature of TiO_2 nanotubes. Mat Sci Semicon Proc 26:107–111
33. Cao SW, Yuan YP, Fang J, Shahjamali MM, Boey FY, Barber J, Loo SCJ, Xue C (2013) In-situ growth of CdS quantum dots on g-C_3N_4 nanosheets for highly efficient photocatalytic hydrogen generation under visible light irradiation. Int J Hydrogen Energy 38:1258–1266.
34. Li X, Liu HL, Luo DL, Li JT, Huang Y, Li HL, Fang YP, Xu Y, Zhu L (2012) Adsorption of CO_2 on heterostructure CdS (Bi_2S_3)/TiO_2 nanotube photocatalysts and their photocatalytic activities in the reduction of CO_2 to methanol under visible light irradiation. Chem Eng J 180:151–158.
35. Gurudayal, Chiam SY, Kumar MH, Bassi PS, Seng HL, Barber J, Wong LH (2014) Improving the efficiency of hematite nanorods for photoelectrochemical water splitting by doping with manganese. ACS Appl Mater Interfaces 6:5852–5859
36. Zhao LD, He JQ, Hao SQ, Wu CI, Hogan TP, Wolverton C, Dravid VP, Kanatzidis MG (2012) Raising the thermoelectric performance of p-Type PbS with endotaxial nanostructuring and valence-band offset engineering using CdS and ZnS. J Am Chem Soc 134:16327–16336.
37. Hernández S, Hidalgo D, Sacco A, Chiodoni A, Lamberti A, Cauda V, Tresso E, Saracco G (2015) Comparison of photocatalytic and transport properties of TiO_2 and ZnO nanostructures for solar-driven water splitting. Phys Chem Chem Phys 17:7775–7786.
38. Zhang C, Fan WQ, Bai HY, Yu XQ, Chen C, Zhang RX, Shi WD (2014) Sandwich-nanostructured NiO-ZnO nanowires @ a-Fe_2O_3 film photoanode with a synergistic effect and p-n junction for efficient photoelectrochemical water splitting. ChemElectroChem 1:2089–2097.
39. Gurudayal, Chee PM, Boix PP, Ge H, Yanan F, Barber J, Wong LH (2015) Core-shell hematite nanorods: a simple method to improve the charge transfer in the photoanode for photoelectrochemical water splitting. ACS Appl Mater Interfaces 7:6852–6859